StyleGAN-XL: Scaling StyleGAN to Large Diverse Datasets

AXEL SAUER, University of Tübingen and Max Planck Institute for Intelligent Systems, Tübingen, Germany
KATJA SCHWARZ, University of Tübingen and Max Planck Institute for Intelligent Systems, Tübingen, Germany
ANDREAS GEIGER, University of Tübingen and Max Planck Institute for Intelligent Systems, Tübingen, Germany

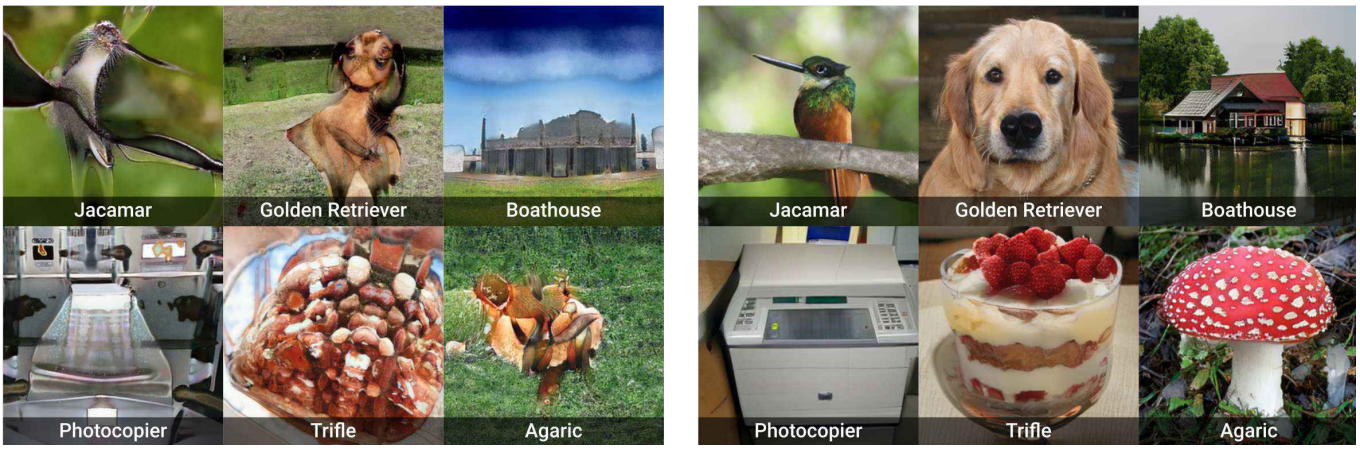

Fig. 1. Class-conditional samples generated by StyleGAN3 (left) and StyleGAN-XL (right) trained on ImageNet at resolution 256^2.

Computer graphics has experienced a recent surge of data-centric approaches for photorealistic and controllable content creation. StyleGAN in particular sets new standards for generative modeling regarding image quality and controllability. However, StyleGAN's performance severely degrades on large unstructured datasets such as ImageNet. StyleGAN was designed for controllability; hence, prior works suspect its restrictive design to be unsuitable for diverse datasets. In contrast, we find the main limiting factor to be the current training strategy. Following the recently introduced Projected GAN paradigm, we leverage powerful neural network priors and a progressive growing strategy to successfully train the latest StyleGAN3 generator on ImageNet. Our final model, StyleGAN-XL, sets a new state-of-the-art on large-scale image synthesis and is the first to generate images at a resolution of 1024^2 at such a dataset scale. We demonstrate that this model can invert and edit images beyond the narrow domain of portraits or specific object classes.

1 INTRODUCTION

Computer graphics has long been concerned with generating photorealistic images at high resolution that allow for direct control over semantic attributes. Until recently, the primary paradigm was to create carefully designed 3D models which are then rendered using realistic camera and illumination models. A parallel line of research approaches the problem from a data-centric perspective. In particular, probabilistic generative models [16, 30, 54, 60] have shifted the paradigm from designing assets to designing training procedures and datasets. Style-based GANs (StyleGANs) are a specific instance of these models, and they exhibit many desirable properties. They achieve high image fidelity [27, 28], fine-grained semantic control [20, 36, 61], and recently alias-free generation enabling realistic animation [26]. Moreover, they reach impressive photorealism on carefully curated datasets, especially of human faces. However, when trained on large and unstructured datasets like ImageNet [12], StyleGANs do not achieve satisfactory results yet. One other problem plaguing data-centric methods, in general, is that they become prohibitively more expensive when scaling to higher resolutions as bigger models are required.

Initially, StyleGAN [27] was proposed to explicitly disentangle factors of variations, allowing for better control and interpolation quality [27]. However, its architecture is more restrictive than a standard generator network [24, 37, 47] which seems to come at a price when training on complex and diverse datasets such as ImageNet. Previous attempts at scaling StyleGAN and StyleGAN2 to ImageNet led to sub-par results [18, 19], giving reason to believe it might be fundamentally limited for highly diverse datasets [19].

BigGAN [5] is the state-of-the-art GAN model for image synthesis on ImageNet. The main factors for BigGANs success are larger batch and model sizes. However, BigGAN has not reached a similar standing as StyleGAN as its performance varies significantly between training runs [25] and as it does not employ an intermediate latent space which is essential for GAN-based image editing [2, 10, 43, 61]. Recently, BigGAN has been superseded in performance by diffusion models [13]. Diffusion models achieve more diverse image synthesis than GANs but are significantly slower during inference and prior work on GAN-based editing is not directly applicable. Following these arguments, successfully training StyleGAN on ImageNet has several advantages over existing methods.

The previously failed attempts at scaling StyleGAN raise the question of whether architectural constraints fundamentally limit style-based generators or if the missing piece is the right training strategy. Recent work by Sauer et al. [52] introduced *Projected GANs* which project generated and real samples into a fixed, pretrained feature space. Rephrasing the GAN setup this way leads to significant improvements in training stability, training time, and data efficiency.

Leveraging the benefits of Projected GAN training might enable scaling StyleGAN to ImageNet. However, as observed by [52], the advantages of Projected GANs only partially extend to StyleGAN on the unimodal datasets they investigated. We study this issue and propose architectural changes to address it. We then design a progressive growing strategy tailored to the latest StyleGAN3. These changes in conjunction with Projected GAN already allow surpassing prior attempts of training StyleGAN on ImageNet. To further improve results, we analyze the pretrained feature network used for Projected GANs and find that the two standard neural architectures for computer vision, CNNs and ViTs [14], significantly improve performance when used jointly. Lastly, we leverage *classifier guidance*, a technique originally introduced for diffusion models to inject additional class-information [13].

Our contributions culminate in a new state-of-the-art on large-scale image synthesis, pushing the performance beyond existing GAN and diffusion models. We showcase inversion and editing for ImageNet classes and find that Pivotal Tuning Inversion (PTI) [49], a powerful new inversion paradigm, combines well with our model and even embeds out-of-domain images smoothly into our learned latent space. Our efficient training strategy allows us to triple the parameters of the standard StyleGAN3 while reaching prior state-of-the-art performance of diffusion models [13] in a fraction of their training time. It further enables us to be the first to demonstrate image synthesis on ImageNet-scale at a resolution of 1024^2 pixels. We will open-source our code and models upon publication. The supplementary video can be found at https://sites.google.com/view/stylegan-xl/.

2 BACKGROUND

We first introduce the main building blocks of our system: the StyleGAN3 generator [26] and Projected GAN's [52] feature projectors and multi-scale discriminators.

StyleGAN. This section describes style-based generators in general with a focus on the latest StyleGAN3 [26]. A StyleGAN generator consists of a mapping network $\mathbf{G}_m$ and a synthesis network $\mathbf{G}_s$. First, $\mathbf{G}_m$ maps a normally distributed latent code $\mathbf{z}$ to a style code $\mathbf{w}$. This style code $\mathbf{w}$ is then used for modulating the convolution kernels of $\mathbf{G}_s$ to control the synthesis process. The synthesis network $\mathbf{G}_s$ of StyleGAN3 starts from a spatial map defined by Fourier features [57, 62]. This input then passes through N layers of convolutions, non-linearities, and upsampling to generate an image. Each non-linearity is wrapped by an upsampling and downsampling operation to prevent aliasing. The low-pass filters used for these operations are carefully designed to balance image quality, antialiasing, and training speed. Concretely, their cutoff and stopband frequencies grow geometrically with network depth, the transition band half-widths are as wide as possible within the limits of the layer sampling rate, and only the last two layers are critically sampled, i.e., the filter cutoff equals the bandlimit. The number of layers N is 14, independent of the final output resolution.

Style mixing and path length regularization are methods for regularizing style-based generators. In style mixing, an image is generated by feeding sampled style codes $\mathbf{w}$ into different layers of $\mathbf{G}_s$ independently. Path length regularization encourages that a step of fixed size in latent space results in a corresponding fixed change in pixel intensity of the generated image [28]. This inductive bias leads to a smoother generator mapping and has several advantages including fewer artifacts, more predictable training behavior, and better inversion.

Progressive growing was introduced by [24] for stable training at high resolutions but [28] found that it can impair shift-equivariance. Karras et al. [26] observe that texture sticking artifacts are caused by a lack of equivariance and carefully design StyleGAN3 to prevent texture sticking. Hence, in this paper, as we build on StyleGAN3, we can revisit the idea of progressive growing to improve convergence speed and synthesis quality.

Projected GAN. The original adversarial game between a generator $\mathbf{G}$ and a discriminator $\mathbf{D}$ can be extended by a set of feature projectors $\{\mathbf{P}_l\}$ [52]. The projectors map real images $\mathbf{x}$ and images generated by $\mathbf{G}$ to the discriminator's input space. The Projected GAN objective is formulated as

$$\min_{\mathbf{G}} \max_{\{\mathbf{D}_l\}} \sum_{l \in \mathcal{L}} \Big(\mathbb{E}_{\mathbf{x}}[\log \mathbf{D}_l(\mathbf{P}_l(\mathbf{x}))] + \mathbb{E}_{\mathbf{z}}[\log(1 - \mathbf{D}_l(\mathbf{P}_l(\mathbf{G}(\mathbf{z}))))] \Big) \tag{1}$$

where $\{\mathbf{D}_l\}$ is a set of independent discriminators operating on different feature projections. The projectors consist of a pretrained feature network $\mathbf{F}$, cross-channel mixing (CCM) and cross-scale mixing (CSM) layers. The purpose of CCM and CSM is to prohibit the discriminators from focusing on only a subset of its input feature space which would result in mode collapse. Both modules employ differentiable random projections that are not optimized during GAN training. CCM mixes features across channels via random 1x1 convolutions, CSM mixes features across scales via residual random 3x3 convolution blocks and bilinear upsampling. The output of CSM is a feature pyramid consisting of four feature maps at different resolutions. Four discriminators operate independently on these feature maps. Each discriminator uses a simple convolutional architecture and spectral normalization [39]. The depth of the discriminator varies depending on its input resolution, i.e., a spatially larger feature map corresponds to a deeper discriminator. Other than spectral normalization, Projected GANs do not use additional regularization such as gradient penalties [38]. Lastly, [52] apply differentiable data-augmentation [66] before $\mathbf{F}$ which improves Projected GAN's performance independent of the dataset size.

Sauer et al. [52] evaluate several combinations of $\mathbf{F}$ and $\mathbf{G}$ and find an EfficientNet-Lite0 [56] and a FastGAN generator [37] to work especially well. When using a StyleGAN generator, they observe that the discriminators can quickly overpower the generator for suboptimal learning rates. The authors suspect that the generator might adapt too slowly due to its design which modulates feature maps with styles learned by a mapping network.

3 SCALING STYLEGAN TO IMAGENET

As mentioned before, StyleGAN has several advantages over existing approaches that work well on ImageNet. But a naïve training strategy does not yield state-of-the-art performance [18, 19]. Our experiments confirm that even the latest StyleGAN3 does not scale

well, see Fig. 1. Particularly at high resolutions, the training becomes unstable, resulting in a high FID. Therefore, our goal is to train a StyleGAN3 generator on ImageNet successfully. Success is defined in terms of sample quality primarily measured by inception score (IS) [51] and diversity measured by Fréchet Inception Distance (FID) [21]. Throughout this section, we gradually introduce changes to the StyleGAN3 baseline (**Config-A**) and track the improvements in Table 1. First, we modify the generator and its regularization losses, adapting the latent space to work well with Projected GAN (**Config-B**) and for the class-conditional setting (**Config-C**). We then revisit progressive growing to improve training speed and performance (**Config-D**). Next, we investigate the feature networks used for Projected GAN training to find a well-suited configuration (**Config-E**). Lastly, we propose classifier guidance for GANs to provide class information via a pretrained classifier (**Config-F**). Our contributions enable us to train a significantly larger model than previously possible while requiring less computation than prior art. Our model is three times larger in terms of depth and parameter count than a standard StyleGAN3. However, to match the prior state-of-the-art performance of ADM [13] at a resolution of 512^2 pixels, training the models on a single NVIDIA Tesla V100 takes 400 days compared to the previously required 1914 V100-days. We refer to our model as **StyleGAN-XL** (Fig. 2).

3.1 Adapting Regularization and Architectures

Training on a diverse and class-conditional dataset makes it necessary to introduce several adjustments to the standard StyleGAN configuration. We construct our generator architecture using layers of StyleGAN3-T, the translational-equivariant configuration of StyleGAN3. In initial experiments, we found the rotational-equivariant StyleGAN3-R to generate overly symmetric images on more complex datasets, resulting in kaleidoscope-like patterns.

Regularization. In GAN training, it is common to use regularization for both, the generator and the discriminator. Regularization improves results on uni-modal datasets like FFHQ [27] or LSUN [63], whereas it can be detrimental on multi-modal datasets [5, 19]. Therefore, we aim to avoid regularization when possible. Karras et al. [26] find style mixing to be unnecessary for the latest StyleGAN3; hence, we also disable it. Path length regularization can lead to poor results on complex datasets [19] and is, per default, disabled for StyleGAN3 [26]. However, path length regularization is attractive as it enables high-quality inversion [28]. We also observe unstable behavior and divergence when using path length regularization in practice. We found that this problem can be circumvented by only applying regularization after the model has been sufficiently trained, i.e., after 200k images. For the discriminator, following [52], we use spectral normalization without gradient penalties. In addition, we blur all images with a Gaussian filter with $\sigma = 2$ pixels for the first $200k$ images. Discriminator blurring has been introduced in [26] for StyleGAN3-R. It prevents the discriminator from focusing on high frequencies early on, which we found beneficial across all settings we investigated.

Low-Dimensional Latent Space. As observed in [52], Projected GANs work better with FastGAN [37] than with StyleGAN. One main difference between these generators is their latent space, StyleGAN's latent space is comparatively high dimensional (FastGAN: $\mathbb{R}^{100}$, BigGAN: $\mathbb{R}^{128}$, StyleGAN: $\mathbb{R}^{512}$). Recent findings indicate that the *intrinsic dimension* of natural image datasets is relatively low [46], ImageNet's dimension estimate is around 40. Accordingly, a latent code of size 512 is highly redundant, making the mapping network's task harder at the beginning of training. Consequently, the generator is slow to adapt and cannot benefit from Projected GAN's speed up. We therefore reduce StyleGAN's latent code $\mathbf{z}$ to 64 and now observe stable training in combination with Projected GAN, resulting in lower FID than the baseline (**Config-B**). We keep the original dimension of the *style code* $\mathbf{w} \in \mathbb{R}^{512}$ to not restrict the model capacity of the mapping network $\mathbf{G}_m$.

Pretrained Class Embeddings. Conditioning the model on class information is essential to control the sample class and improve overall performance. A class-conditional variant of StyleGAN was first proposed in [25] for CIFAR10 [32] where a one-hot encoded label is embedded into a 512-dimensional vector and concatenated with $\mathbf{z}$. For the discriminator, class information is projected onto the last discriminator layer [39]. We observe that **Config-B** tends to generate similar samples per class. To quantify mode coverage, we leverage the recall metric [33] and find that **Config-B** achieves a low recall of 0.004. We hypothesize that the class embeddings collapse when training with Projected GAN. Therefore, to prevent this collapse, we aim to ease optimization of the embeddings via pretraining. We extract and spatially pool the lowest resolution features of an Efficientnet-lite0 [56] and calculate the mean per ImageNet class. The network has a low channel count to keep the embedding dimension small, following the arguments of the previous section. The embedding passes through a linear projection to match the size of $\mathbf{z}$ to avoid an imbalance. Both $\mathbf{G}_m$ and $\mathbf{D}_i$ are conditioned on the embedding. During GAN training, the embedding and the linear projection are optimized to allow specialization. Using this configuration, we observe that the model generates diverse samples per class, and recall increases to 0.15 (**Config-C**). Note that for all configurations in this ablation, we restrict the training time to 15 V-100 *days*. Hence, the absolute recall is markedly lower compared to the fully trained models. Conditioning a GAN on pretrained features was also recently investigated by [6]. In contrast to our approach, Casanova et al. [6] condition on specific *instances*, instead of learning a general class embedding.

3.2 Reintroducing Progressive Growing

Progressively growing the output resolution of a GAN was introduced by [24] for fast and more stable training. The original formulation adds layers during training to both $\mathbf{G}$ and $\mathbf{D}$ and gradually fades in their contribution. However, in a later work, it was discarded [28] as it can contribute to texture sticking artifacts. Recent work by Karras et al. [26] finds that the primary cause of these artifacts is aliasing, so they redesign each layer of StyleGAN to prevent it. This motivates us to reconsider progressive growing with a carefully crafted strategy that aims to suppress aliasing as best as possible. Training first on very low resolutions, as small as 16^2 pixels, enables us to break down the daunting task of training on high-resolution ImageNet into smaller subtasks. This idea is in line with the latest

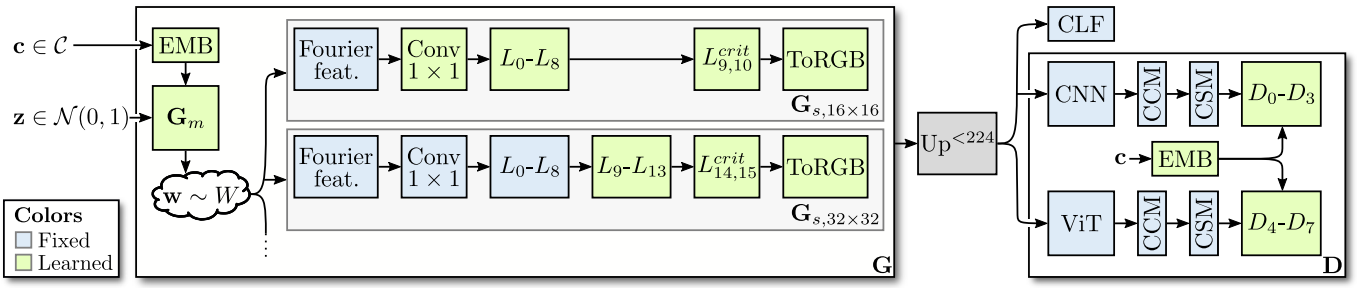

Fig. 2. **Training StyleGAN-XL**. We feed a latent code $\mathbf{z}$ and class label $\mathbf{c}$ to the pretrained embedding and the mapping network $\mathbf{G}_m$ to generate style codes $\mathbf{w}$. The codes modulate the convolutions of the synthesis network $\mathbf{G}_s$. During training, we gradually add layers to double the output resolution for each stage of the progressive growing schedule. We only train the latest layers while keeping the others fixed. The synthesized image is upsampled when smaller than 224^2 and passed through a CNN and a ViT and respective feature mixing blocks (CCM+CSM). At higher resolutions, the CNN receives the unaltered image while the ViT receives a downsampled input to keep memory requirements low but still utilize its global feedback. Finally, we apply eight independent discriminators on the resulting multi-scale feature maps. The image is also fed to classifier CLF for classifier guidance.

	Configuration	FID ↓	IS ↑
A	StyleGAN3	53.57	15.30
B	+ Projected GAN & small $\mathbf{z}$	22.98	57.62
C	+ Pretrained embeddings	20.91	35.79
D	+ Progressive growing	19.51	35.74
E	+ ViT & CNN as $\mathbf{F}_{1,2}$	12.43	56.72
F	+ CLF guidance (StyleGAN-XL)	**12.24**	**86.21**

Model		Type		Objective		FID ↓	IS ↑
$\mathbf{F}_1$	$\mathbf{F}_2$	$\mathbf{F}_1$	$\mathbf{F}_2$	$\mathbf{F}_1$	$\mathbf{F}_2$		
EffNet		CNN		Class		19.51	35.74
EffNet	ResNet50	CNN	CNN	Class	Class	16.16	49.13
EffNet	ResNet50	CNN	CNN	Class	Self	18.53	38.26
EffNet	DeiT-M	CNN	ViT	Class	Class	**12.43**	**56.72**

Table 1. **Ablation Study on ImageNet** 128^2. Left: Results for different configurations after training for 15 V100-days. Right: Comparing combinations of different feature networks $\mathbf{F}$. Beginning from the base configuration using an EfficientNet-lite0 (EffNet), we add a second $\mathbf{F}$ with varying architecture type and pretraining objective (*Class*: Classification, *Self*: MoCo-v2 [9]).

work on diffusion models [13, 22, 42, 50]. They observe considerable improvements in FID on ImageNet when using a two-stage model, i.e., stacking an independent low-resolution model and an upsampling model to generate the final image.

Commonly, GANs follow a rigid sampling rate progression, i.e., at each resolution, there is a fixed amount of layers followed by an upsampling operation using fixed filter parameters. StyleGAN3 does not follow such a progression. Instead, the layer count is set to 14, independent of the output resolution, and the filter parameters of up- and downsampling operations are carefully designed for antialiasing under the given configuration. The last two layers are critically sampled to generate high-frequency details. When adding layers for the subsequent highest resolution, discarding the previously critically sampled layers is crucial as they would introduce aliasing when used as intermediate layers [26, 28]. Furthermore, we adjust the filter parameters of the added layers to adhere to the flexible layer specification of [26]; we refer to the supplementary for details. In contrast to [24] we do not add layers to the discriminator. Instead, to fully utilize the pretrained feature network $\mathbf{F}$, we upsample both data and synthesized images to $\mathbf{F}$'s training resolution (224^2 pixels) when training on smaller images.

We start progressive growing at a resolution of 16^2 using 11 layers. Every time the resolution increases, we cut off 2 layers and add 7 new ones. Empirically, fewer layers result in worse performance; adding more leads to increased overhead and diminishing returns. For the final stage at 1024^2, we add only 5 layers as the last two are not discarded. This amounts to 39 layers at the maximum resolution of 1024^2. Instead of a fixed growing schedule, each stage is trained until FID stops decreasing. We find it beneficial to use a large batch size of 2048 on lower resolution (16^2 to 64^2), similar to [5]. On higher resolutions, smaller batch sizes suffice (128^2 to 256^2: 256, 512^2 to 1024^2: 128). Once new layers are added, the lower resolution layers remain fixed to prevent mode collapse.

In our ablation study, FID improves only slightly (**Config-D**) compared to **Config-C**. However, the main advantage can be seen at high resolutions, where progressive growing drastically reduces training time. At resolution 512^2, we reach the prior state-of-the-art (FID = 3.85) after 2 V100-days. This reduction is in contrast to other methods such as ADM, where doubling the resolution from 256^2 to 512^2 pixels corresponds to increasing training time from 393 to 1914 V100-days to find the best performing model[1]. As our aim is not to introduce texture sticking artifacts, we measure *EQ-T*, a metric for determining translation equivariance [26], where higher is better. **Config-C** yields *EQ-T* = 55, while **Config-D** attains *EQ-T* = 48. This only slight reduction in equivariance shows that **Config-D** restricts aliasing almost as well as a configuration without growing. For context, architectures with aliasing yield *EQ-T* ∼ 15.

3.3 Exploiting Multiple Feature Networks

An ablation study conducted in [52] finds that most pretrained feature networks $\mathbf{F}$ perform similarly in terms of FID when used

[1]Note that these settings are not directly comparable as the stem of our model is pretrained, but the values should give a general sense of the order of magnitude.

for Projected GAN training regardless of training data, pretraining objective, or network architecture. However, the study does not answer if combining several **F** is advantageous. Starting from the standard configuration, an EfficientNet-lite0, we add a second **F** to inspect the influence of its pretraining objective (classification or self-supervision) and architecture (CNN or Vision Transformer (ViT) [14]). The results in Table 1 show that an additional CNN leads to slightly lower FID. Combining networks with different pretraining objectives does not offer benefits over using two classifier networks. However, combining an EfficientNet with a ViT improves performance significantly. This result corroborates recent results in neural architecture literature, which find that supervised and self-supervised representations are similar [17], whereas ViTs and CNNs learn different representations [48]. Combining both architectures appears to have complementary effects for Projected GANs. We do not see significant improvements when adding more networks; hence, **Config-E** uses the combination of EfficientNet [56] and DeiT-M [58].

3.4 Classifier Guidance for GANs

Dhariwal and Nichol [13] introduced classifier guidance to inject class information into diffusion models. Classifier guidance modifies each diffusion step at time step t by adding the gradients of a pretrained classifier $\nabla_{\mathbf{x}_t} \log p_\phi(\mathbf{c}|x_t, t)$. The best results are obtained when applying guidance on class-conditional models and scaling the classifier gradients by a constant $\lambda > 1$. This successful combination indicates that our model may also profit from classifier guidance, even though we already supply class information via embeddings.

We first pass the generated image $\mathbf{x}$ through a pretrained classifier CLF to predict the class label c_i. We then add a cross-entropy loss $\mathcal{L}_{CE} = -\sum_{i=0}^{C} c_i \log CLF(x_i)$ as an additional term to the generator loss and scale this term by a constant λ. For the classifier, we use DeiT-S [58], which exhibits strong classification performance while not adding much overhead to the training. Similar to [13], we observe a significant improvement in IS, indicating an increase in sample quality (**Config-F**). We find $\lambda = 8$ to work well empirically. Classifier guidance only works well on higher resolutions ($> 32^2$); otherwise, it leads to mode collapse. This is in contrast to [13] who exclusively guide their low-resolution model. The difference stems from how guidance is applied: we use it for model training, whereas [13] guide the sampling process.

4 RESULTS

In this section, we first compare StyleGAN-XL to the state-of-the-art approaches for image synthesis on ImageNet. We then evaluate the inversion and editing capabilities of StyleGAN-XL. As described above, we scale our model to a resolution of 1024^2 pixels, which no prior work has attempted so far on ImageNet. The resolution of most images in ImageNet is lower. We therefore preprocess the data with a super-resolution network [35], see supplementary.

4.1 Image Synthesis

Both our work and [13] use classifier networks to guide the generator. To ensure the models are not inadvertently optimizing for FID and IS, which also utilize a classifier network, we propose random-FID (rFID). For rFID, we calculate the Fréchet distance in the `pool_3` layer of a randomly initialized inception network [55]. The efficacy of random features for evaluating generative models has been demonstrated in [40]. Furthermore, we report sFID [41] to assess the spatial structure of generated samples. Lastly, sample fidelity and diversity are evaluated via precision and recall [33] complementing FID and IS.

In Table 2, we compare StyleGAN-XL to the currently strongest GAN model (BigGAN-deep [5]) and diffusion models (CDM [22], ADM [13]) on ImageNet. The values for ADM are calculated with and without additional methods (Upsampling **U** and Classifier Guidance **G**). Both BigGAN and StyleGAN-XL allow for the truncation trick, i.e., drawing a latent code from a truncated sampling space. A lower truncation ψ increases sample quality while lowering sample diversity, resulting in an FID vs. IS tradeoff [5]. We find that StyleGAN-XL substantially outperforms all baselines across all resolutions in FID, sFID, rFID, and IS. An exception is precision and recall. According to recall, StyleGAN-XL's sample diversity lies between BigGAN and ADM, making progress in closing the gap between these model types. StyleGAN-XL's increase in diversity comes at the price of individual sample quality measured by precision, where BigGAN is the best among all compared approaches. Interestingly, StyleGAN-XL attains high diversity across all resolutions, which can be attributed to our progressive growing strategy. Furthermore, this strategy enables to scale to megapixel resolution successfully. Training at 1024^2 for a single V100-day yields a noteworthy FID of 4.3. At this resolution, we do not compare to baselines because of resource constraints as they are prohibitively expensive to train. Fig. 3 visualizes generated samples at increasing resolutions.

4.2 Inversion and Manipulation

GAN-editing methods first *invert* a given image into latent space, i.e., find a style code w that reconstructs the image as faithful as possible when passed through $\mathbf{G}_s$. Then, $\mathbf{w}$ can be manipulated to achieve semantically meaningful edits.

Inversion. Standard approaches for inverting $\mathbf{G}_s$ use either latent optimization [1, 11, 28] or an encoder [3, 44, 59]. A common way to achieve low reconstruction error is to use an extended definition of the latent space: $\mathcal{W}+$. For $\mathcal{W}+$ a separate $\mathbf{w}$ is chosen for each layer of $\mathbf{G}_s$. However, as highlighted by [59], this extended definition achieves higher reconstruction quality in exchange for lower editability. Therefore, [59] carefully design an encoder to maintain editability by mapping to regions of $\mathcal{W}+$ that are close to the original distribution of $\mathcal{W}$. We follow [28] and use the original latent space $\mathcal{W}$. We find that StyleGAN-XL already achieves satisfactory inversion results using basic latent optimization. For inversion on the ImageNet validation set at 512^2, StyleGAN-XL yields PSNR = 13.5 on average, improving over BigGAN at PSNR = 10.8. Besides better pixel-wise reconstruction, StyleGAN-XL's inversions are semantically closer to the target images. We measure the FID between reconstructions and targets, and StyleGAN-XL attains FID = 21.7 while BigGAN reaches FID = 47.5. Fig. 4 shows qualitative results. For implementation details and additional metrics, we refer to the supplementary.

Model	FID ↓	sFID ↓	rFID ↓	IS ↑	Pr ↑	Rec ↑	Model	FID ↓	sFID ↓	rFID ↓	IS ↑	Pr ↑	Rec ↑
Resolution 128^2							**Resolution** 256^2						
BigGAN-deep ($\psi = 1.0$) [5]	6.02	7.18	6.09	145.83	0.82	0.36	StyleGAN2 [18]	49.20					
BigGAN-deep ($\psi = 0.1$) [5]	29.46	54.50	12.07	261.46	**0.86**	0.00	BigGAN-deep ($\psi = 1.0$) [5]	6.95	7.36	75.24	202.65	0.86	0.24
CDM [22]	3.52			128.80			BigGAN-deep ($\psi = 0.1$) [5]	27.00	69.88	19.66	313.67	**0.88**	0.00
ADM [13]	5.91	5.09	13.29	93.31	0.71	**0.57**	CDM [22]	4.88			158.70		
ADM-G [13]	2.97	5.09	3.80	141.37	0.75	0.56	ADM [13]	10.94	6.02	125.78	100.98	0.72	**0.50**
StyleGAN-XL ($\psi = 1.0$)	**2.54**	**4.02**	**1.31**	180.58	0.75	0.46	ADM-G-U [13]	3.94	6.14	11.86	215.84	0.81	0.47
StyleGAN-XL ($\psi = 0.1$)	28.29	47.44	64.85	**369.98**	**0.86**	0.00	**StyleGAN-XL** ($\psi = 1.0$)	**3.26**	**4.22**	**4.28**	225.27	0.74	0.45
							StyleGAN-XL ($\psi = 0.1$)	25.84	47.58	63.88	**413.94**	0.78	0.00
Resolution 512^2							**Resolution** 1024^2						
BigGAN-deep ($\psi = 1.0$) [5]	8.43	8.13	312.00	177.90	0.85	0.25	**StyleGAN-XL** ($\psi = 1.0$)	**3.71**	**4.54**	**518.61**	195.66	0.74	**0.38**
BigGAN-deep ($\psi = 0.1$) [5]	27.30	70.30	169.15	291.80	**0.87**	0.00	**StyleGAN-XL** ($\psi = 0.1$)	26.45	49.17	1522.00	**367.97**	**0.80**	0.00
ADM [13]	23.24	10.19	561.32	58.06	0.70	0.39							
ADM-G-U [13]	3.85	5.86	210.83	221.72	0.81	**0.45**							
StyleGAN-XL ($\psi = 1.0$)	**3.58**	**4.35**	**48.03**	219.77	0.73	0.43							
StyleGAN-XL ($\psi = 0.1$)	25.21	47.73	263.50	**409.12**	0.75	0.00							

Table 2. **Image Synthesis on ImageNet**. Empty cells indicate that the model was not available and the respective metric not evaluated in the original work. A lower truncation ψ increases sample quality while lowering sample diversity. StyleGAN-XL outperforms all baselines in FID, sFID, rFID, and IS. According to recall and precision, StyleGAN-XL attains high sample diversity while slightly decreasing sample quality compared to the GAN baseline BigGAN-deep.

Given the results above, it is also possible to further refine the obtained reconstructions. Roich et al. [49] recently introduced pivotal tuning inversion (PTI). PTI uses an initial inverted style code as a pivot point around which the generator is finetuned. Additional regularization prevents altering the generator output far from the pivot. Combining PTI with StyleGAN-XL allows us to invert both in-domain (ImageNet validation set) and out-of-domain images almost precisely. At the same time, the generator output remains perceptually smooth, see Fig. 5.

Image Manipulation. Given the inverted images, we can leverage GAN-based editing methods to manipulate the style code $\mathbf{w}$. In Fig. 6 (Left), we first invert a given source image via latent space optimization. We then apply different manipulation directions obtained by GANspace [20] and StyleMC [31]. Prior work [23] also investigates in-plane translation. This operation can be directly defined in the input grid of StyleGAN-XL. The input grid also allows to perform extrapolation by increasing the grid size.

An inherent property of StyleGAN is the ability of style mixing by supplying the style codes of two samples to different layers of $\mathbf{G}_s$, generating a hybrid image. This hybrid takes on different semantic properties of both inputs. Style mixing is commonly employed for instances of a single domain, i.e., combining two human portraits. StyleGAN-XL inherits this ability and, to a certain extent, even generates out-of-domain combinations between different classes, akin to counterfactual images presented in [53]. This technique works best for aligned samples, similar to StyleGAN's originally favored setting, FFHQ. Curated examples are shown in Fig. 6 (Right).

5 LIMITATIONS AND FUTURE WORK

Our contributions allow StyleGAN to accomplish state-of-the-art high-resolution image synthesis on ImageNet. Exploring new editing methods and dataset generation [7, 34] using StyleGAN-XL are exciting future avenues. Furthermore, future work may tackle an even larger megapixel dataset. However, a larger yet diverse dataset is not available so far. Current large-scale, high-resolution datasets are of single object classes or contain many similar images [15, 45, 65]. In the following, we discuss some limitations of the current model which should be addressed in the future.

Architectural Limitations. First, StyleGAN-XL is three times larger than StyleGAN3, constituting a higher computational overhead when used as a starting point for finetuning. Therefore, it will be worth exploring GAN distillation methods [8] that trade-off performance for model size. Second, StyleGAN-XL uses translation-equivariant layers of StyleGAN3-T. As described above, StyleGAN3-R tends to produce overly symmetrical images and adds significant computational overhead. Finding a more efficient rotational-equivariant architecture is an important future direction. Lastly, we find StyleGAN3, and consequently, StyleGAN-XL, harder to edit, e.g., high-quality edits via $\mathcal{W}$ are noticeably easier to achieve with StyleGAN2. As already observed in [26], StyleGAN3's semantic controllability is reduced for the sake of equivariance. However, techniques using the *StyleSpace* [61], e.g. StyleMC [31], tend to yield better results in our experiments confirming the findings of concurrent work by Alaluf et al. [4]. Furthermore, we remark that for applications where equivariance is not essential, our framework can easily be used with StyleGAN2 layers instead.

Drawbacks Compared to Diffusion Models. Low data coverage is a known problem of GANs, and StyleGAN-XL makes notable headway on this issue. However, StyleGAN-XL is still outperformed by diffusion models regarding data coverage. Furthermore, similar to [5], classes of unaligned humans appear harder to model for a GAN. For such classes, ADM [13] generates more convincing human faces than BigGAN [5] or StyleGAN-XL, see supplementary. Whether the points above are a general limitation of GANs remains an interesting open question for future research.

Fig. 3. **Samples at Different Resolutions Using the Same w**. The samples are generated by the models obtained during progressive growing. We upsample all images to 1024^2 using nearest-neighbor interpolation for visualization purposes. Zooming in is recommended.

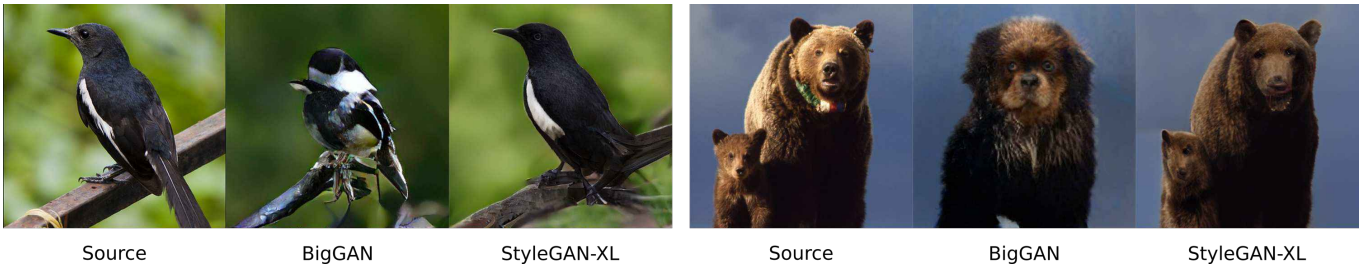

Fig. 4. **Inversion of a Given Source Image**. For BigGAN, we invert to its latent space **z**, for StyleGAN-XL we invert to style codes **w**.

Fig. 5. **Interpolations**. StyleGAN-XL generates smooth interpolations between samples of different classes (Row 1 & Row 2). PTI [49] allows inverting to the latent space with low distortion (outermost image, Row 3 & Row 4), and consistently embeds out-of-domain inputs, such as the one on the bottom right.

Fig. 6. **Image Manipulation**. Left: Given a source image of the ImageNet validation set, we first invert and then edit the image. The top row uses PTI [49] for inversion and edits the image with a direction discovered by GANspace [20]. The second row also uses PTI for inversion and extrapolates by providing a bigger input grid. The bottom row uses standard inversion, as we find that PTI does not mix well with the semantic edits of StyleMC [31]. The image was manipulated to show "a happy teddy bear". Right: Given two images, we can mix their styles. This methods works for samples of the same or similar classes, and to a certain extent, for distant classes. For this experiment, we utilize random samples instead of inversions.

ACKNOWLEDGMENTS

We acknowledge the financial support by the BMWi in the project KI Delta Learning (project number 19A19013O). Andreas Geiger was supported by the ERC Starting Grant LEGO-3D (850533). We would like to thank Kashyap Chitta, Michael Niemeyer, and Božidar Antić for proofreading. Lastly, we would like to thank Vanessa Sauer for her general support.

REFERENCES

[1] Rameen Abdal, Yipeng Qin, and Peter Wonka. 2019. Image2StyleGAN: How to Embed Images Into the StyleGAN Latent Space?. In *Proc. of the IEEE International Conf. on Computer Vision (ICCV)*. 4431–4440. https://doi.org/10.1109/ICCV.2019.00453

[2] Rameen Abdal, Peihao Zhu, Niloy J. Mitra, and Peter Wonka. 2021. StyleFlow: Attribute-conditioned Exploration of StyleGAN-Generated Images using Conditional Continuous Normalizing Flows. *ACM Trans. on Graphics* 40, 3 (2021), 21:1–21:21. https://doi.org/10.1145/3447648

[3] Yuval Alaluf, Or Patashnik, and Daniel Cohen-Or. 2021. ReStyle: A Residual-Based StyleGAN Encoder via Iterative Refinement. *Proc. of the IEEE International Conf. on Computer Vision (ICCV)* abs/2104.02699 (2021). https://arxiv.org/abs/2104.02699

[4] Yuval Alaluf, Or Patashnik, Zongze Wu, Asif Zamir, Eli Shechtman, Dani Lischinski, and Daniel Cohen-Or. 2022. Third Time's the Charm? Image and Video Editing with StyleGAN3. *arXiv.org* abs/2201.13433 (2022). https://arxiv.org/abs/2201.13433

[5] Andrew Brock, Jeff Donahue, and Karen Simonyan. 2019. Large Scale GAN Training for High Fidelity Natural Image Synthesis. In *Proc. of the International Conf. on Learning Representations (ICLR)*. OpenReview.net. https://openreview.net/forum?id=B1xsqj09Fm

[6] Arantxa Casanova, Marlène Careil, Jakob Verbeek, Michal Drozdzal, and Adriana Romero-Soriano. 2021. Instance-Conditioned GAN. In *Advances in Neural Information Processing Systems (NeurIPS)*.

[7] Lucy Chai, Jun-Yan Zhu, Eli Shechtman, Phillip Isola, and Richard Zhang. 2021. Ensembling With Deep Generative Views. In *Proc. IEEE Conf. on Computer Vision and Pattern Recognition (CVPR)*. Computer Vision Foundation / IEEE, 14997–15007. https://openaccess.thecvf.com/content/CVPR2021/html/Chai_Ensembling_With_Deep_Generative_Views_CVPR_2021_paper.html

[8] Ting-Yun Chang and Chi-Jen Lu. 2020. TinyGAN: Distilling BigGAN for Conditional Image Generation. In *Proc. of the Asian Conf. on Computer Vision (ACCV) (Lecture Notes in Computer Science, Vol. 12625)*, Hiroshi Ishikawa, Cheng-Lin Liu, Tomás Pajdla, and Jianbo Shi (Eds.). 509–525. https://doi.org/10.1007/978-3-030-69538-5_31

[9] Xinlei Chen, Haoqi Fan, and Ross Girshick Kaiming He. 2020. Improved baselines with momentum contrastive learning. arxiv.org:2003.04297

[10] Edo Collins, Raja Bala, Bob Price, and Sabine Süsstrunk. 2020. Editing in Style: Uncovering the Local Semantics of GANs. In *Proc. IEEE Conf. on Computer Vision and Pattern Recognition (CVPR)*. Computer Vision Foundation / IEEE, 5770–5779. https://doi.org/10.1109/CVPR42600.2020.00581

[11] Antonia Creswell and Anil Anthony Bharath. 2019. Inverting the Generator of a Generative Adversarial Network. *IEEE Trans. Neural Networks Learn. Syst.* 30, 7 (2019), 1967–1974. https://doi.org/10.1109/TNNLS.2018.2875194

[12] Jia Deng, Wei Dong, Richard Socher, Li-Jia Li, Kai Li, and Li Fei-Fei. 2009. ImageNet: A large-scale hierarchical image database. In *Proc. IEEE Conf. on Computer Vision and Pattern Recognition (CVPR)*. IEEE Computer Society, 248–255. https://doi.org/10.1109/CVPR.2009.5206848

[13] Prafulla Dhariwal and Alex Nichol. 2021. Diffusion Models Beat GANs on Image Synthesis. (2021).

[14] Alexey Dosovitskiy, Lucas Beyer, Alexander Kolesnikov, Dirk Weissenborn, Xiaohua Zhai, Thomas Unterthiner, Mostafa Dehghani, Matthias Minderer, Georg Heigold, Sylvain Gelly, Jakob Uszkoreit, and Neil Houlsby. 2021. An Image is Worth 16x16 Words: Transformers for Image Recognition at Scale. In *Proc. of the International Conf. on Learning Representations (ICLR)*. OpenReview.net. https://openreview.net/forum?id=YicbFdNTTy

[15] Andreas Fregin, Julian Müller, Ulrich Krebel, and Klaus Dietmayer. 2018. The DriveU Traffic Light Dataset: Introduction and Comparison with Existing Datasets. In *Proc. IEEE International Conf. on Robotics and Automation (ICRA)*. IEEE, 3376–3383. https://doi.org/10.1109/ICRA.2018.8460737

[16] Ian J. Goodfellow, Jean Pouget-Abadie, Mehdi Mirza, Bing Xu, David Warde-Farley, Sherjil Ozair, Aaron C. Courville, and Yoshua Bengio. 2014. Generative Adversarial Nets. In *Advances in Neural Information Processing Systems (NeurIPS)*, Zoubin Ghahramani, Max Welling, Corinna Cortes, Neil D. Lawrence, and Kilian Q. Weinberger (Eds.). 2672–2680. https://proceedings.neurips.cc/paper/2014/hash/5ca3e9b122f61f8f06494c97b1afccf3-Abstract.html

[17] Tom George Grigg, Dan Busbridge, Jason Ramapuram, and Russ Webb. 2021. Do Self-Supervised and Supervised Methods Learn Similar Visual Representations? arxiv.org:2110.00528

[18] Timofey Grigoryev, Andrey Voynov, and Artem Babenko. 2022. When, Why, and Which Pretrained GANs Are Useful?. In *Proc. of the International Conf. on Learning Representations (ICLR)*. https://openreview.net/forum?id=4Ycr8oeCoIh

[19] Gwern. 2020. *Making Anime Faces with StyleGAN*. Retrieved January 16, 2022 from https://www.gwern.net/Faces#stylegan2-ext-modifications/

[20] Erik Härkönen, Aaron Hertzmann, Jaakko Lehtinen, and Sylvain Paris. 2020. GANSpace: Discovering Interpretable GAN Controls. In *Advances in Neural Information Processing Systems (NeurIPS)*. https://proceedings.neurips.cc/paper/2020/hash/6fe43269967adbb64ec6149852b5cc3e-Abstract.html

[21] Martin Heusel, Hubert Ramsauer, Thomas Unterthiner, Bernhard Nessler, and Sepp Hochreiter. 2017. GANs Trained by a Two Time-Scale Update Rule Converge to a Local Nash Equilibrium. In *Advances in Neural Information Processing Systems (NeurIPS)*. 6626–6637. https://proceedings.neurips.cc/paper/2017/hash/8a1d694707eb0fefe65871369074926d-Abstract.html

[22] Jonathan Ho, Chitwan Saharia, William Chan, David J. Fleet, Mohammad Norouzi, and Tim Salimans. 2021. Cascaded Diffusion Models for High Fidelity Image Generation. arxiv.org:2106.15282

[23] Ali Jahanian, Lucy Chai, and Phillip Isola. 2020. On the "steerability" of generative adversarial networks. In *Proc. of the International Conf. on Learning Representations (ICLR)*. OpenReview.net. https://openreview.net/forum?id=HylsTT4FvB

[24] Tero Karras, Timo Aila, Samuli Laine, and Jaakko Lehtinen. 2018. Progressive Growing of GANs for Improved Quality, Stability, and Variation. In *Proc. of the International Conf. on Learning Representations (ICLR)*. OpenReview.net. https://openreview.net/forum?id=Hk99zCeAb

[25] Tero Karras, Miika Aittala, Janne Hellsten, Samuli Laine, Jaakko Lehtinen, and Timo Aila. 2020. Training Generative Adversarial Networks with Limited Data. In *Advances in Neural Information Processing Systems (NeurIPS)*. https://proceedings.neurips.cc/paper/2020/hash/8d30aa96e72440759f74bd2306c1fa3d-Abstract.html

[26] Tero Karras, Miika Aittala, Samuli Laine, Erik Härkönen, Janne Hellsten, Jaakko Lehtinen, and Timo Aila. 2021. Alias-Free Generative Adversarial Networks. In *Advances in Neural Information Processing Systems (NeurIPS)*.

[27] Tero Karras, Samuli Laine, and Timo Aila. 2019. A Style-Based Generator Architecture for Generative Adversarial Networks. In *Proc. IEEE Conf. on Computer Vision and Pattern Recognition (CVPR)*. Computer Vision Foundation / IEEE, 4401–4410. https://doi.org/10.1109/CVPR.2019.00453

[28] Tero Karras, Samuli Laine, Miika Aittala, Janne Hellsten, Jaakko Lehtinen, and Timo Aila. 2020. Analyzing and Improving the Image Quality of StyleGAN. In *Proc. IEEE Conf. on Computer Vision and Pattern Recognition (CVPR)*. Computer Vision Foundation / IEEE, 8107–8116. https://doi.org/10.1109/CVPR42600.2020.00813

[29] Diederik P. Kingma and Jimmy Ba. 2015. Adam: A Method for Stochastic Optimization. In *Proc. of the International Conf. on Learning Representations (ICLR)*.

[30] Diederik P. Kingma and Prafulla Dhariwal. 2018. Glow: Generative Flow with Invertible 1x1 Convolutions. In *Advances in Neural Information Processing Systems (NeurIPS)*, Samy Bengio, Hanna M. Wallach, Hugo Larochelle, Kristen Grauman, Nicolò Cesa-Bianchi, and Roman Garnett (Eds.). 10236–10245. https://proceedings.neurips.cc/paper/2018/hash/d139db6a236200b21cc7f752979132d0-Abstract.html

[31] Umut Kocasari, Alara Dirik, Mert Tiftikci, and Pinar Yanardag. 2022. StyleMC: Multi-Channel Based Fast Text-Guided Image Generation and Manipulation. *Proc. of the IEEE Winter Conference on Applications of Computer Vision (WACV)* (2022). https://arxiv.org/abs/2112.08493

[32] Alex Krizhevsky, Geoffrey Hinton, et al. 2009. Learning multiple layers of features from tiny images. (2009).

[33] Tuomas Kynkäänniemi, Tero Karras, Samuli Laine, Jaakko Lehtinen, and Timo Aila. 2019. Improved Precision and Recall Metric for Assessing Generative Models. In *Advances in Neural Information Processing Systems (NeurIPS)*. https://proceedings.neurips.cc/paper/2019/hash/0234c510bc6d908b28c70ff313743079-Abstract.html

[34] Daiqing Li, Huan Ling, Seung Wook Kim, Karsten Kreis, Adela Barriuso, Sanja Fidler, and Antonio Torralba. 2022. BigDatasetGAN: Synthesizing ImageNet with Pixel-wise Annotations. *arXiv.org* (2022). https://arxiv.org/abs/2201.04684

[35] Jingyun Liang, Jiezhang Cao, Guolei Sun, Kai Zhang, Luc Van Gool, and Radu Timofte. 2021. SwinIR: Image Restoration Using Swin Transformer. In *Proc. of the IEEE International Conf. on Computer Vision (ICCV) Workshops*. IEEE, 1833–1844. https://doi.org/10.1109/ICCVW54120.2021.00210

[36] Huan Ling, Karsten Kreis, Daiqing Li, Seung Wook Kim, Antonio Torralba, and Sanja Fidler. 2021. EditGAN: High-Precision Semantic Image Editing. *arXiv.org* abs/2111.03186 (2021). https://arxiv.org/abs/2111.03186

[37] Bingchen Liu, Yizhe Zhu, Kunpeng Song, and Ahmed Elgammal. 2021. Towards Faster and Stabilized GAN Training for High-fidelity Few-shot Image Synthesis. In *Proc. of the International Conf. on Learning Representations (ICLR)*. OpenReview.net. https://openreview.net/forum?id=1Fqg133qRaI

[38] Lars M. Mescheder, Andreas Geiger, and Sebastian Nowozin. 2018. Which Training Methods for GANs do actually Converge?. In *Proc. of the International Conf. on Machine learning (ICML) (Proceedings of Machine Learning Research, Vol. 80)*. PMLR, 3478–3487. http://proceedings.mlr.press/v80/mescheder18a.html

[39] Takeru Miyato, Toshiki Kataoka, Masanori Koyama, and Yuichi Yoshida. 2018. Spectral Normalization for Generative Adversarial Networks. In *Proc. of the International Conf. on Learning Representations (ICLR)*. OpenReview.net. https://openreview.net/forum?id=B1QRgziT-

[40] Muhammad Ferjad Naeem, Seong Joon Oh, Youngjung Uh, Yunjey Choi, and Jaejun Yoo. 2020. Reliable Fidelity and Diversity Metrics for Generative Models. In *Proceedings of the 37th International Conference on Machine Learning, ICML 2020, 13-18 July 2020, Virtual Event (Proceedings of Machine Learning Research, Vol. 119)*. 7176–7185. http://proceedings.mlr.press/v119/naeem20a.html

[41] Charlie Nash, Jacob Menick, Sander Dieleman, and Peter W. Battaglia. 2021. Generating images with sparse representations. In *Proc. of the International Conf. on Machine learning (ICML)*. http://proceedings.mlr.press/v139/nash21a.html

[42] Alexander Quinn Nichol and Prafulla Dhariwal. 2021. Improved Denoising Diffusion Probabilistic Models. In *Proc. of the International Conf. on Machine learning (ICML) (Proceedings of Machine Learning Research, Vol. 139)*. PMLR, 8162–8171. http://proceedings.mlr.press/v139/nichol21a.html

[43] Or Patashnik, Zongze Wu, Eli Shechtman, Daniel Cohen-Or, and Dani Lischinski. 2021. StyleCLIP: Text-Driven Manipulation of StyleGAN Imagery. In *Proc. of the IEEE International Conf. on Computer Vision (ICCV)*. 2085–2094.

[44] Guim Perarnau, Joost van de Weijer, Bogdan C. Raducanu, and Jose M. Álvarez. 2016. Invertible Conditional GANs for image editing. *arXiv.org* abs/1611.06355 (2016). http://arxiv.org/abs/1611.06355

[45] Etienne Perot, Pierre de Tournemire, Davide Nitti, Jonathan Masci, and Amos Sironi. 2020. Learning to Detect Objects with a 1 Megapixel Event Camera. In *Advances in Neural Information Processing Systems (NeurIPS)*. https://proceedings.neurips.cc/paper/2020/hash/c213877427b46fa96cff6c39e837ccee-Abstract.html

[46] Phillip Pope, Chen Zhu, Ahmed Abdelkader, Micah Goldblum, and Tom Goldstein. 2021. The Intrinsic Dimension of Images and Its Impact on Learning. In *Proc. of the International Conf. on Learning Representations (ICLR)*. OpenReview.net. https://openreview.net/forum?id=XJk19XzGq2J

[47] Alec Radford, Luke Metz, and Soumith Chintala. 2016. Unsupervised Representation Learning with Deep Convolutional Generative Adversarial Networks. In *Proc. of the International Conf. on Learning Representations (ICLR)*, Yoshua Bengio and Yann LeCun (Eds.). http://arxiv.org/abs/1511.06434

[48] Maithra Raghu, Thomas Unterthiner, Simon Kornblith, Chiyuan Zhang, and Alexey Dosovitskiy. 2021. Do Vision Transformers See Like Convolutional Neural Networks?. In *Advances in Neural Information Processing Systems (NeurIPS)*.

[49] Daniel Roich, Ron Mokady, Amit H. Bermano, and Daniel Cohen-Or. 2021. Pivotal Tuning for Latent-based Editing of Real Images. *arXiv.org* (2021). https://arxiv.org/abs/2106.05744

[50] Chitwan Saharia, Jonathan Ho, William Chan, Tim Salimans, David J. Fleet, and Mohammad Norouzi. 2021. Image Super-Resolution via Iterative Refinement. arxiv.org:2104.07636

[51] Tim Salimans, Ian J. Goodfellow, Wojciech Zaremba, Vicki Cheung, Alec Radford, and Xi Chen. 2016. Improved Techniques for Training GANs. In *Advances in Neural Information Processing Systems (NeurIPS)*. 2226–2234. https://proceedings.neurips.cc/paper/2016/hash/8a3363abe792db2d8761d6403605aeb7-Abstract.html

[52] Axel Sauer, Kashyap Chitta, Jens Müller, and Andreas Geiger. 2021. Projected GANs Converge Faster. In *Advances in Neural Information Processing Systems (NeurIPS)*.

[53] Axel Sauer and Andreas Geiger. 2021. Counterfactual Generative Networks. In *Proc. of the International Conf. on Learning Representations (ICLR)*. OpenReview.net. https://openreview.net/forum?id=BXewfAYMmJw

[54] Jiaming Song, Chenlin Meng, and Stefano Ermon. 2021. Denoising Diffusion Implicit Models. In *Proc. of the International Conf. on Learning Representations (ICLR)*. https://openreview.net/forum?id=St1giarCHLP

[55] Christian Szegedy, Wei Liu, Yangqing Jia, Pierre Sermanet, Scott E. Reed, Dragomir Anguelov, Dumitru Erhan, Vincent Vanhoucke, and Andrew Rabinovich. 2015. Going deeper with convolutions. In *Proc. IEEE Conf. on Computer Vision and Pattern Recognition (CVPR)*. IEEE Computer Society, 1–9. https://doi.org/10.1109/CVPR.2015.7298594

[56] Mingxing Tan and Quoc V. Le. 2019. EfficientNet: Rethinking Model Scaling for Convolutional Neural Networks. In *Proc. of the International Conf. on Machine learning (ICML) (Proceedings of Machine Learning Research, Vol. 97)*, Kamalika Chaudhuri and Ruslan Salakhutdinov (Eds.). PMLR, 6105–6114. http://proceedings.mlr.press/v97/tan19a.html

[57] Matthew Tancik, Pratul P. Srinivasan, Ben Mildenhall, Sara Fridovich-Keil, Nithin Raghavan, Utkarsh Singhal, Ravi Ramamoorthi, Jonathan T. Barron, and Ren Ng. 2020. Fourier Features Let Networks Learn High Frequency Functions in Low Dimensional Domains. In *Advances in Neural Information Processing Systems (NeurIPS)*. https://proceedings.neurips.cc/paper/2020/hash/55053683268957697aa39fba6f231c68-Abstract.html

[58] Hugo Touvron, Matthieu Cord, Matthijs Douze, Francisco Massa, Alexandre Sablayrolles, and Hervé Jégou. 2021. Training data-efficient image transformers & distillation through attention. In *Proc. of the International Conf. on Machine learning (ICML) (Proceedings of Machine Learning Research, Vol. 139)*. PMLR, 10347–10357. http://proceedings.mlr.press/v139/touvron21a.html

[59] Omer Tov, Yuval Alaluf, Yotam Nitzan, Or Patashnik, and Daniel Cohen-Or. 2021. Designing an Encoder for StyleGAN Image Manipulation. *ACM Trans. on Graphics* 40, 4 (2021). https://doi.org/10.1145/3450626.3459838

[60] Aäron van den Oord, Oriol Vinyals, and Koray Kavukcuoglu. 2017. Neural Discrete Representation Learning. In *Advances in Neural Information Processing Systems (NeurIPS)*, Isabelle Guyon, Ulrike von Luxburg, Samy Bengio, Hanna M. Wallach, Rob Fergus, S. V. N. Vishwanathan, and Roman Garnett (Eds.). 6306–6315. https://proceedings.neurips.cc/paper/2017/hash/7a98af17e63a0ac09ce2e96d03992fbc-Abstract.html

[61] Zongze Wu, Dani Lischinski, and Eli Shechtman. 2021. StyleSpace Analysis: Disentangled Controls for StyleGAN Image Generation. In *Proc. IEEE Conf. on Computer Vision and Pattern Recognition (CVPR)*. Computer Vision Foundation / IEEE, 12863–12872. https://openaccess.thecvf.com/content/CVPR2021/html/Wu_StyleSpace_Analysis_Disentangled_Controls_for_StyleGAN_Image_Generation_CVPR_2021_paper.html

[62] Rui Xu, Xintao Wang, Kai Chen, Bolei Zhou, and Chen Change Loy. 2021. Positional Encoding As Spatial Inductive Bias in GANs. In *Proc. IEEE Conf. on Computer Vision and Pattern Recognition (CVPR)*. Computer Vision Foundation / IEEE, 13569–13578. https://openaccess.thecvf.com/content/CVPR2021/html/Xu_Positional_Encoding_As_Spatial_Inductive_Bias_in_GANs_CVPR_2021_paper.html

[63] Fisher Yu, Yinda Zhang, Shuran Song, Ari Seff, and Jianxiong Xiao. 2015. LSUN: Construction of a Large-scale Image Dataset using Deep Learning with Humans in the Loop. arxiv.org:1506.03365

[64] Richard Zhang, Phillip Isola, Alexei A. Efros, Eli Shechtman, and Oliver Wang. 2018. The Unreasonable Effectiveness of Deep Features as a Perceptual Metric. In *Proc. IEEE Conf. on Computer Vision and Pattern Recognition (CVPR)*. Computer Vision Foundation / IEEE Computer Society, 586–595. https://doi.org/10.1109/CVPR.2018.00068

[65] Xucong Zhang, Seonwook Park, Thabo Beeler, Derek Bradley, Siyu Tang, and Otmar Hilliges. 2020. ETH-XGaze: A Large Scale Dataset for Gaze Estimation Under Extreme Head Pose and Gaze Variation. In *Proc. of the European Conf. on Computer Vision (ECCV) (Lecture Notes in Computer Science, Vol. 12350)*. Springer, 365–381. https://doi.org/10.1007/978-3-030-58558-7_22

[66] Shengyu Zhao, Zhijian Liu, Ji Lin, Jun-Yan Zhu, and Song Han. 2020. Differentiable Augmentation for Data-Efficient GAN Training. In *Advances in Neural Information Processing Systems (NeurIPS)*. https://proceedings.neurips.cc/paper/2020/hash/55479c55ebd1efd3ff125f1337100388-Abstract.html

Fig. 7. **Imagenet Classes Containing Humans**. Samples for BigGAN and ADM are taken from [13].

Appendix

In this supplemental document, we elaborate on increasing the resolution of ImageNet to one megapixel, compare to the baseline on a class containing humans, and specify the implementation details of our approach. The supplemental video shows additional samples and interpolations. We use the same mathematical notation as in the paper.

A PREPROCESSING IMAGENET

An initial challenge is the lack of high-resolution data; the mean resolution of ImageNet is 469×387. Similar to the procedure used for generating CelebA-HQ[24], we preprocess the whole dataset with SwinIR-Large [35], a recent model for real-world image super-resolution. Of course, a trivial way of achieving good performance on this dataset would be to draw samples from a 256^2 generative model and passing it through SwinIR. However, SwinIR adds significant computational overhead as it is 60 times slower than our upsampling stack. Furthermore, this way, StyleGAN-XL's weights can be used for initialization when finetuning on other high-resolution datasets. Lastly, combining StyleGAN-XL and SwinIR would impair translation equivariance.

B CLASSES OF UNALIGNED HUMANS

As mentioned in section 5, we observe that ADM [13] generates more convincing human faces than StyleGAN-XL and BigGAN. Both GANs can synthesize realistic faces; however, the main challenge in this setting is that the dataset is unstructured, and the humans are not aligned. Brock et al. [5] remarked the particular challenge of classes containing details to which human observers are more sensitive. We show examples in Fig. 7.

C IMPLEMENTATION DETAILS

Inversion. Following [28], we use basic latent optimization in $\mathcal{W}$ for inversion. Given a target image, we first compute its average style code $\bar{\mathbf{w}}$ by running 10000 random latent codes $\mathbf{z}$ and target specific class samples $\mathbf{c}$ through the mapping network. As the class label of the target image is unknown, we pass it to a pretrained classifier. We then use the classifier logits as a multinomial distribution to sample $\mathbf{c}$. In our experiments, we use Deit-M [58] as a classifier, but other choices are possible. At the beginning of optimization , we initialize $\mathbf{w} = \bar{\mathbf{w}}$. The components of $\mathbf{w}$ are the only trainable parameters. The optimization runs for 1000 iterations using the Adam optimizer [29] with default parameters. We optimize the LPIPS [64] distance between the target image and the generated image. For StyleGAN-XL, the maximum learning rate is $\lambda_{max} = 0.05$. It is ramped up from zero linearly during the first 50 iterations and ramped down to zero using a cosine schedule during the last 250 iterations. For BigGAN, we empirically found $\lambda_{max} = 0.001$ and a ramp-down over the last 750 iterations to yield the best results. All inversion experiments are performed at resolution 512^2 and computed on $5k$ images (10% of the validation set). We report the results in Table 3.

Model	MSE ↓	PSNR ↑	SSIM ↑	FID ↓
BigGAN	0.095	10.85	0.26	47.48
StyleGAN-XL	**0.056**	**13.45**	**0.33**	**21.73**

Table 3. **Inversion Results.** The metrics are computed between the inversions obtained by the model and the reconstruction targets.

Training StyleGAN3 on ImageNet. For training StyleGAN3, we use the official PyTorch implementation[2]. The results in Fig. 1 are computed with the StyleGAN3-R configuration on resolution 256^2 until the discriminator has seen 10 million images. We find that StyleGAN3-R and StyleGAN3-T converge to similar FID without any changes to their training paradigm. The run with the best FID score was selected from three runs with different random seeds. We use a channel base of 16384 and train on 8 GPUs with total batch size 256, $\gamma = 0.256$. The remaining settings are chosen according to the default configuration of the code release. For the ablation study in Table 1, we use the StyleGAN3-T configuration as baseline since StyleGAN-XL builds upon the translational-equivariant layers of StyleGAN3. We train on 4 GPUs with total batch size 256 and batch size 32 per GPU, $\gamma = 0.25$, and disable augmentation.

Training & Evaluation. For all our training runs, we do not use data amplification via *x-flips* following [27]. Furthermore, we evaluate all metrics using the official StyleGAN3 codebase. For the baseline values in Table 2, we report the numbers of [13]. The official codebase of ADM[3] provides files containing 50k samples for ADM and BigGAN. We utilize the provided samples to compute rFID. In addition, we recompute precision and recall for all baselines, as [13] compute these metrics between 10k real samples and 50k generated samples. We follow the original formulation of [33] and use 50k real and 50k generated samples.

Layer configurations. We start progressive growing at resolution 16^2 using 11 layers. The layer specifications are computed according to [26] and remain fixed for the remaining training. For the next stage, at resolution 32^2, we discard the last 2 layers and add 7 new ones. The specifications for the new layers are computed according to [26] for a model with resolution 32^2 and 16 layers. Continuing this strategy up to resolution 1024^2 yields the flexible layer specification of StyleGAN-XL in Fig. 8.

[2] https://github.com/NVlabs/stylegan3.git
[3] https://github.com/openai/guided-diffusion

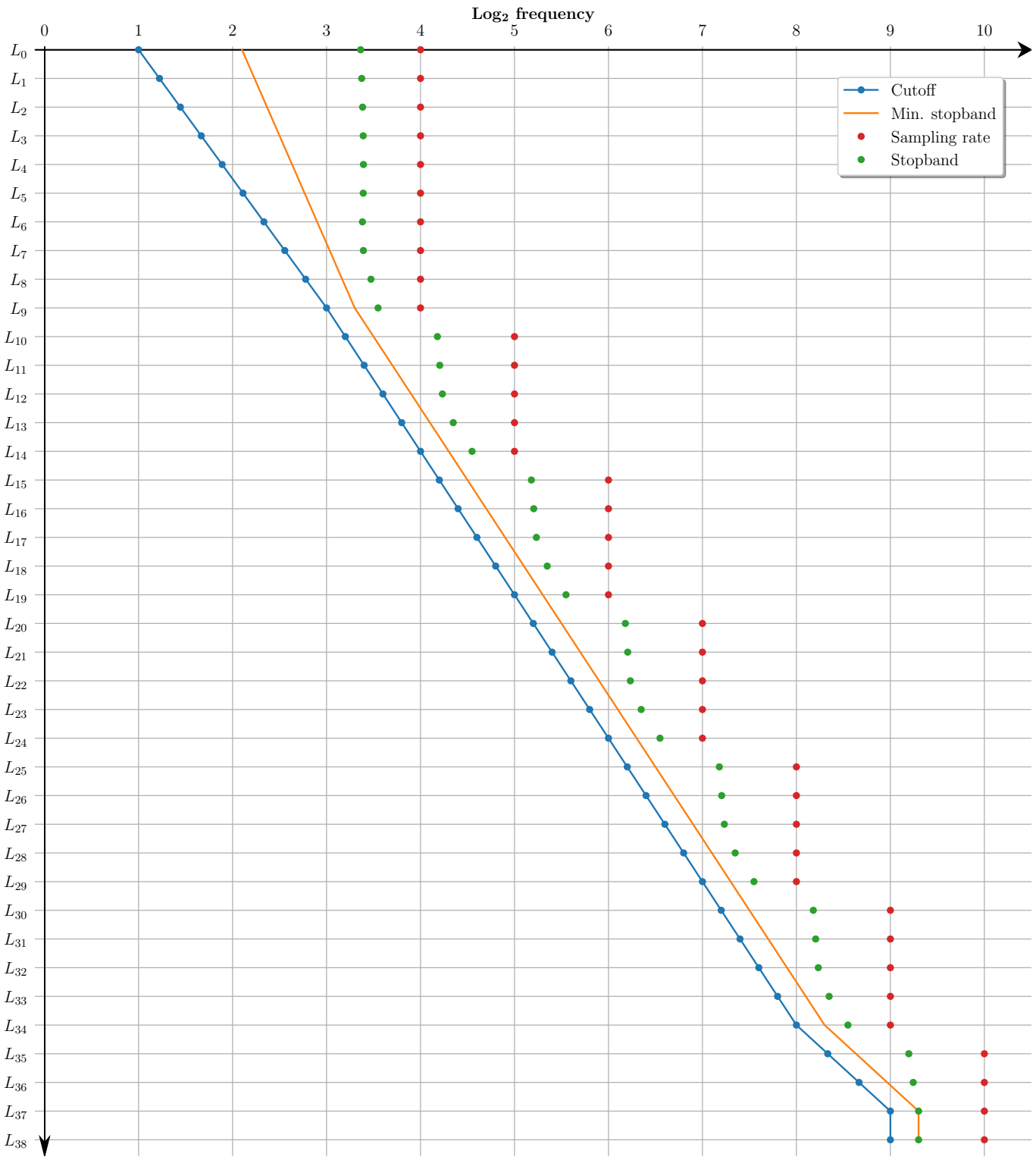

Fig. 8. **Flexible Layer Specification of Stylegan-XL**. StyleGAN-XL consists of 39 layers at resolution 1024^2. Cutoff (blue) and minimum acceptable stopband frequency (orange) obey geometric progression over the layers; sampling rate (red) and actual stopband (green) are computed according to our design constraints.